PHYSICAL REVIEW D **86,** 094032 (2012)

Exploring criticality in the QCD-like two quark flavor models

Vivek Kumar Tiwari*

Department of Physics, University of Allahabad, Allahabad 211002, India

(Received 12 August 2012; published 20 November 2012)

The critical end point (CEP) and the critical behavior in its vicinity have been explored in the two-flavor effective chiral models with and without the presence of an effective Polyakov loop potential. The tricritical point (TCP) in the massless chiral limit has been located on the phase diagram in the μ and T plane for the Polyakov loop-extended quark-meson model (PQM) and the pure quark-meson model, which become effective quantum chromodynamics (QCD)-like models due to the proper accounting of fermionic vacuum loop contributions in the effective potential. The proximity of the TCP to the QCD critical end point (CEP) has been quantified in the phase diagram. The critical region around the CEP has been obtained in both the presence and absence of fermionic vacuum-loop contributions in the effective potentials of the PQM and quark-meson models. The contours of appropriately normalized constant quark number susceptibility and scalar susceptibility have been plotted around the CEP in different model scenarios. These contours determine the shape of the critical region and facilitate comparisons between different models such that the influence of the fermionic vacuum term and the Polyakov loop potential on the critical behavior around the CEP can be ascertained in qualitative as well as quantitative terms. Critical exponents resulting from the divergence of quark number susceptibility at the CEP have been calculated and compared with those in different model scenarios. The possible influence of the TCP on the critical behavior around the CEP has also been discussed. The temperature variation of σ and π meson masses at $\mu = 0$, $\mu = \mu_{\mathrm{CEP}}$, and $\mu > \mu_{\mathrm{CEP}}$ has been shown and compared with that seen in different model scenarios and the emerging mass degeneration trend in the σ and π meson mass variations has been inferred as the chiral-symmetry restoration takes place at higher temperatures.

DOI: 10.1103/PhysRevD.86.094032 PACS numbers: 12.38.Aw, 11.10.Wx, 12.38.Lg, 12.39.Fe

I. INTRODUCTION

Under the extreme conditions of high temperature and/or density, normal hadronic matter undergoes a phase transition, where the individual hadrons dissolve into their quark and gluon constituents and produce a collective form of matter known as the quark-gluon plasma (QGP) [1–4]. The study of the different aspects of this phase transition is a challenging task because quantum chromodynamics (QCD)—the theory of strong interactions—becomes nonperturbative in the low-energy limit. However, the QCD vacuum reveals itself through the process of spontaneous chiral symmetry breaking and the phenomenon of color confinement.

The QCD Lagrangian is known to have global $SU_{L+R}(N_f) \times SU_{L-R}(N_f)$ symmetry for N_f flavors of massless quarks. The formation of a chiral condensate in the low-energy hadronic vacuum of QCD leads to the spontaneous breaking of the axial (A = R − L) part of this symmetry, known as the chiral symmetry, and one gets $(N_f^2 - 1)$ massless Goldstone bosons according to Goldstone's theorem. Since quarks are not actually massless, the chiral symmetry of the QCD Lagrangian is explicitly broken and massless modes become pseudo-Goldstone bosons after acquiring mass. Nevertheless, the observed lightness of pions in nature suggests that we have an approximate chiral symmetry for QCD with two flavors of light u and d quarks. In the opposite limit of infinitely heavy quarks, QCD becomes a pure $SU(N_c)$ gauge theory which remains invariant under the global $Z(N_c)$ center symmetry of the color gauge group. The center symmetry—a symmetry of the hadronic vacuum—is spontaneously broken in the high temperature/density regime of the QGP. The expectation value of the Wilson line (Polyakov loop) is related to the free energy of a static color charge. It vanishes in the confining phase (as the quark has infinite free energy) and becomes finite in the deconfined phase. Hence the Polyakov loop serves as the order parameter of the confinement-deconfinement phase transition [5]. Even though the center symmetry is always broken with the inclusion of dynamical quarks in the system, one can regard the Polyakov loop as an approximate order parameter because it is a good indicator of a rapid crossover in the confinement-deconfinement transition [6,7].

Lattice QCD simulations (see, e.g., Refs. [8–18]) give us important information and insights regarding various aspects of the QGP transition, such as the restoration of chiral symmetry in QCD, the order of the confinement-deconfinement phase transition, the richness of the QCD phase structure, and phase diagram mapping. Since lattice calculations are technically involved and various issues are not conclusively settled within the lattice community, one resorts to the calculations within the ambit of phenomenological models developed in terms of effective degrees of

*vivekkrt@gmail.com

freedom. These models serve to complement the lattice simulations and give much needed insight about the regions of the phase diagram that are inaccessible to lattice simulations.

The construction and mapping of the phase diagram in the quark chemical potential and temperature plane is the primary challenge presented to the experimental and theoretical QGP community. On the temperature axis, the chiral transition at zero quark chemical potential with almost physical quark masses has been shown to be a crossover in recent lattice QCD simulations [13,19]. Effective chiral model studies [20] predict a first-order phase transition at lower temperatures on the chemical potential axis. Thus the existence of a critical end point (CEP) has been suggested in the phase diagram based on model studies [21–23] together with the inputs from lattice simulations [10–12]. The first-order transition line starting from the lowest temperature on the chemical potential axis terminates at the CEP, which is a genuine singularity of the QCD free energy. Here the phase transition turns second-order and its criticality belongs to the three-dimensional Ising universality class [24–27]. The precise location of the CEP is highly sensitive to the value of the strange quark mass. Lattice QCD predictions at nonzero chemical potential are much more difficult due to the QCD action becoming complex on account of the fermion sign problem [9]. There is evidence for a CEP at finite μ [10,11] from a Taylor expansion of the QCD pressure around $\mu = 0$. In another lattice study, finite chemical potential extrapolations provide some limitations and can rule out the existence of a CEP for small μ/T ratios [28]; however, even this exotic scenario can be turned around if the critical surface in the mass-chemical potential plane suffers a backbending at finite μ, as shown in Refs. [29,30]. In the chiral limit of zero up and down quark masses, the chiral phase transition is of second order at zero μ and the static critical behavior is expected to fall in the universality class of the O(4) spin model in three dimensions [20]. Thus the existence of a CEP for the actual two-quark-flavor QCD implies that two-flavor massless QCD has a tricritical point (TCP) at which the second-order O(4) line of critical points ends.

Experimental signatures encoding the singular behavior of thermodynamic quantities in the vicinity of the critical point have already been suggested [31]. These are related to chemical potential and temperature fluctuations in event-by-event fluctuations of various particle multiplicities [32]. In the center-of-mass energy scans, an increase and then a decrease in the number of fluctuations of pions and protons should be observed as one crosses the critical point. If the signals are not washed out due to the expansion of the colliding system, the critical point might be located in the phase diagram by the observation of nonmonotonic behavior of number fluctuations in its vicinity [33]. Recently, the beam energy scan program dedicated to the search for critical points has begun at the Relativistic Heavy Ion Collider [34]. The Compressed Baryonic Matter experiment (GSI-Darmstadt) at the Facility for Antiproton and Ion Research and the Nuclotron-based Ion Collider Facility at the Joint Institute for Nuclear Research will also be looking for the signatures of a critical end point. Characteristic signatures of the conjectured CEP for experiments have been discussed in Refs. [35–37].

Recently, effective chiral models, such as the linear sigma models [38–44], the quark-meson (QM) models (see, e.g., Refs. [29,30,45–53]), and Nambu-Jona-Lasinio (NJL)-type models [45,54–57] were extended to combine the features of a confinement-deconfinement transition together with that of a chiral symmetry breaking-restoring phase transition. The chiral order parameter and Polyakov loop order parameter were simultaneously coupled to the quark degrees of freedom in these models. Thus Polyakov loop-augmented NJL (PNJL) models [58–76], Polyakov loop-augmented linear sigma models, and Polyakov loop-extended quark-meson (PQM) models [77–85] have facilitated the investigation of the full QCD thermodynamics and phase structure at zero and finite quark chemical potential, and it has been shown that the bulk thermodynamics of the effective models agrees well with the lattice QCD data. The issue of the location of the CEP in the phase diagram together with the extent of criticality around it is also being actively pursued in a variety of effective model studies [24,25,86–93]. The critical region around the CEP is not point-like, but rather has a much richer structure. The estimation of the size of the critical region is especially important for future experimental searches for the CEP in heavy ion collision experiments.

In the no-sea mean-field approximations, an ultraviolet divergent part of the fermionic vacuum loop contribution to the grand potential were until recently frequently neglected in the QM/PQM model calculations [29,45,46,51,56]. Because of this, the phase transition on the temperature axis at $\mu = 0$ for the two-flavor QM model becomes first-order in the chiral limit of massless quarks, and one does not find a TCP on the phase diagram. Recently, Skokov *et al.* in Ref. [84] addressed this issue by incorporating appropriately renormalized fermionic vacuum fluctuations in the thermodynamic potential of the QM model at zero chemical potential, which becomes an effective QCD-like model as it is then able to reproduce the expected second-order chiral phase transition at $\mu = 0$ from the universality arguments [20] for the two massless flavors of QCD. The fermionic vacuum correction and its influence has also been investigated in earlier works [94–97]. In a recent work [98], we generalized the proper accounting of renormalized fermionic vacuum fluctuations in the two-flavor PQM model to the nonzero chemical potentials and found that the position of the CEP shifts to a significantly higher chemical potential in the μ and T plane of the phase diagram due to the influence of a

fermionic vacuum term in our calculations using a PQM model with a vacuum term (PQMVT). Very recently, Schaefer *et al.* [99] worked out the size of the critical region around the CEP in a three-flavor (2 + 1) PQM model where the cutoff-independent renormalization of fermionic vacuum fluctuations has been considered. They calculated critical exponents and higher-order non-Gaussian moments to identify the fluctuations in particle multiplicities. The effect of fermionic vacuum fluctuations was also investigated in another recent 2 + 1-quark-flavor study [100]. Since the criticality around the CEP is influenced by the presence of the strange quark, it is important to have a two-flavor calculation in the same model in order to facilitate the comparison with the corresponding size of the critical region and the nature of the criticality obtained in 2 + 1-flavor QM/PQM model studies.

In this paper, we will calculate the phase diagram in the massless chiral limit and locate the tricritical point (TCP) in the μ and T plane for the PQMVT model and the QM model with a vacuum term (QMVT) which have become QCD-like in the presence of a fermionic vacuum term and which yield the second-order transition at $\mu = 0$ on the temperature axis. Further, we will be investigating the size and extent of the critical region around the CEP in the phase diagram calculated in the two-flavor QM/PQM models with and without the effect of fermionic vacuum fluctuations in the grand potential. We will be plotting the contours of appropriately normalized constant quark number susceptibility and scalar susceptibility around the CEP in different model scenarios. In order to investigate the qualitative and quantitative effect of a fermionic vacuum term and the Polyakov loop potential on the critical behavior around the CEP, we will compare the shape of these contours as obtained in different model calculations. Further, we compute and compare the critical exponents resulting from the divergence of quark number susceptibility at the CEP in different model scenarios. The possible influence of the TCP on the critical behavior around the CEP will also be discussed. Finally, we will plot the temperature variation of σ and π meson masses at $\mu = 0$, $\mu = \mu_{\mathrm{CEP}}$, and $\mu > \mu_{\mathrm{CEP}}$ in different model scenarios and compare the emerging mass degeneration trend in the σ and π meson mass variations as the chiral symmetry is restored at higher temperatures.

In the presentation of this paper, we recapitulate the formulation of the two-quark flavor PQM model in Sec. II. The thermodynamic grand potential and the choice of the Polyakov loop potential is discussed in Sec. II A. In Sec. II B we give a brief description of the appropriate renormalization of fermionic vacuum loop contributions and explain how the new model parameters are obtained in vacuum when a renormalized vacuum term is added to the effective potential. Section III explores the proximity of the QCD tricritical point to the critical end point and the detailed structure of the phase diagram for the QMVT and PQMVT models where the effect of fermionic vacuum terms has been taken care of in the QM and PQM models. The structure of the phase diagram for the QM and PQM models and the location of the critical end point will also be presented to facilitate the comparison. Section III A investigates the extent of criticality around the CEP where contours of constant baryon number susceptibility ratios and constant scalar susceptibility ratios are presented in the μ and T plane, and a comparison of all four models (QM, PQM, QMVT, and PQMVT) is made. The critical exponents for the criticality around the CEP in all four models is discussed in the Sec. III B. Section III C presents the temperature variation of σ and π meson masses at $\mu = 0$, $\mu = \mu_{\mathrm{CEP}}$, and $\mu > \mu_{\mathrm{CEP}}$. Here we also present a detailed comparison of the emerging mass degeneration trends in the σ and π meson mass variations in different model scenarios as the chiral-symmetry restoration takes place at higher temperatures. Finally, Sec. IV presents a summary together with the conclusion. The first and second partial derivatives of $\mathcal{U}_{\log}$ and $\Omega^{\mathrm{T}}_{\mathrm{q\bar{q}}}$ with respect to temperature and chemical potential are evaluated in Appendix A of Ref. [98].

II. MODEL FORMULATION

We will be working in the two-flavor quark-meson linear sigma model, which has been combined with the Polyakov loop potential [77]. In this model, quarks coming in two flavors are coupled to the $SU_L(2) \times SU_R(2)$-symmetric four mesonic fields σ and $\vec{\pi}$ together with the spatially constant temporal gauge field represented by the Polyakov loop potential. The Polyakov loop field $\Phi(\vec{x})$ is defined as the thermal expectation value of the color trace of the Wilson loop in the temporal direction:

$$\Phi = \frac{1}{N_c}\,\mathrm{Tr}_c L, \qquad \Phi^* = \frac{1}{N_c}\,\mathrm{Tr}_c L^\dagger, \tag{1}$$

where L(x) is a matrix in the fundamental representation of the $SU_c(3)$ color gauge group,

$$L(\vec{x}) = \mathcal{P}\exp\left[i\int_0^\beta d\tau A_0(\vec{x},\tau)\right]. \tag{2}$$

Here $\mathcal{P}$ is the path ordering, A_0 is the temporal component of the Euclidean vector field, and $\beta = T^{-1}$ [5].

The model Lagrangian is written in terms of quarks, mesons, couplings, and the Polyakov loop potential $\mathcal{U}(\Phi, \Phi^*, T)$:

$$\mathcal{L}_{\mathrm{PQM}} = \mathcal{L}_{\mathrm{QM}} - \mathcal{U}(\Phi, \Phi^*, T), \tag{3}$$

where the Lagrangian in the quark-meson linear sigma model is

$$\mathcal{L}_{\mathrm{QM}} = \bar{q}_f[i\gamma^\mu D_\mu - g(\sigma + i\gamma_5\vec{\tau}\cdot\vec{\pi})]q_f + \mathcal{L}_m. \tag{4}$$

The coupling of quarks with the uniform temporal background gauge field is affected by the following

replacement: $D_\mu = \partial_\mu - iA_\mu$ and $A_\mu = \delta_{\mu 0} A_0$ (Polyakov gauge), where $A_\mu = g_s A_\mu^a \lambda^a/2$, g_s is the $SU_c(3)$ gauge coupling, λ_a are Gell-Mann matrices in the color space (a runs from $1 \ldots 8$), $q_f = (u, d)^T$ denotes the quarks coming in two flavors and three colors, g is the flavor-blind Yukawa coupling that couples the two flavors of quarks with the four mesons [one scalar (σ, $J^P = 0^+$) and three pseudoscalars ($\vec{\pi}$, $J^P = 0^-$)].

The quarks have no intrinsic mass but become massive after spontaneous chiral symmetry breaking because of the nonvanishing vacuum expectation value of the chiral condensate. The mesonic part of the Lagrangian has the following form:

$$\mathcal{L}_m = \frac{1}{2}(\partial_\mu \sigma)^2 + \frac{1}{2}(\partial_\mu \vec{\pi})^2 - U(\sigma, \vec{\pi}). \tag{5}$$

The pure mesonic potential is given by the expression

$$U(\sigma, \vec{\pi}) = \frac{\lambda}{4}(\sigma^2 + \vec{\pi}^2 - \upsilon^2)^2 - h\sigma. \tag{6}$$

Here λ is the quartic coupling of the mesonic fields, υ is the vacuum expectation value of the scalar field when chiral symmetry is explicitly broken, and $h = f_\pi m_\pi^2$.

A. The Polyakov loop potential and the thermodynamic grand potential

The effective potential $\mathcal{U}(\Phi, \Phi^*, T)$ is constructed such that it reproduces the thermodynamics of pure glue theory on the lattice for temperatures up to about twice the deconfinement phase transition temperature. In this work, we are using a logarithmic form of Polyakov loop effective potential [60]. The results produced by this potential are known to be fitted well to the lattice results. This potential is given by the following expression:

$$\frac{\mathcal{U}_{\log}(\Phi, \Phi^*, T)}{T^4} = -\frac{a(T)}{2}\Phi^*\Phi + b(T)\ln[1 - 6\Phi^*\Phi + 4(\Phi^{*3} + \Phi^3) - 3(\Phi^*\Phi)^2], \tag{7}$$

where the temperature dependent coefficients are

$$a(T) = a_0 + a_1\left(\frac{T_0}{T}\right) + a_2\left(\frac{T_0}{T}\right)^2, \qquad b(T) = b_3\left(\frac{T_0}{T}\right)^3.$$

The parameters of Eq. (7) are

$$a_0 = 3.51, \qquad a_1 = -2.47,$$
$$a_2 = 15.2, \qquad b_3 = -1.75.$$

The critical temperature for the deconfinement phase transition $T_0 = 270$ MeV is fixed for a pure gauge Yang Mills theory. In the presence of dynamical quarks T_0 is directly linked to the mass scale Λ_{QCD}, the parameter which has a flavor and chemical potential dependence in full dynamical QCD, and $T_0 \rightarrow T_0(N_f, \mu)$ [77,85]. For our numerical calculations in this paper, we have taken a fixed $T_0 = 208$ MeV for two flavors of quarks.

In the mean-field approximation, the thermodynamic grand potential for the PQM model is given as [77]

$$\Omega_{\mathrm{MF}}(T, \mu; \sigma, \Phi, \Phi^*) = \mathcal{U}(T; \Phi, \Phi^*) + U(\sigma) + \Omega_{q\bar{q}}(T, \mu; \sigma, \Phi, \Phi^*). \tag{8}$$

Here, we have written the vacuum expectation values $\langle\sigma\rangle = \sigma$ and $\langle\vec{\pi}\rangle = 0$.

The quark/antiquark contribution in the presence of the Polyakov loop reads

$$\Omega_{q\bar{q}}(T, \mu; \sigma, \Phi, \Phi^*) = \Omega_{q\bar{q}}^{\mathrm{vac}} + \Omega_{q\bar{q}}^{\mathrm{T}} = -2N_f \int \frac{d^3p}{(2\pi)^3}\{N_c E_q \theta(\Lambda^2 - \vec{p}^2) + T[\ln g_q^+ + \ln g_q^-]\}. \tag{9}$$

The first term of Eq. (9) denotes the fermion vacuum contribution, regularized by the ultraviolet cutoff Λ. In the second term g_q^+ and g_q^- have been defined after taking the trace over the color space:

$$g_q^+ = [1 + 3\Phi e^{-E_q^+/T} + 3\Phi^* e^{-2E_q^+/T} + e^{-3E_q^+/T}], \tag{10}$$

$$g_q^- = [1 + 3\Phi^* e^{-E_q^-/T} + 3\Phi e^{-2E_q^-/T} + e^{-3E_q^-/T}]. \tag{11}$$

Here we use the notation $E_q^\pm = E_q \mp \mu$, with E_q being the single-particle energy of the quark/antiquark,

$$E_q = \sqrt{p^2 + m_q^2}, \tag{12}$$

where the constituent quark mass $m_q = g\sigma$ is a function of the chiral condensate. In vacuum $\sigma(0, 0) = \sigma_0 = f_\pi = 93.0$ MeV.

B. The renormalized vacuum term and model parameters

The fermion vacuum loop contribution can be obtained by appropriately renormalizing the first term of Eq. (9) using the dimensional regularization scheme, as done in Ref. [84]. A brief description of the essential steps is given below.

The fermion vacuum term is just the one-loop zero-temperature effective potential at lowest order [101]:

$$\Omega_{q\bar{q}}^{\mathrm{vac}} = -2N_f N_c \int \frac{d^3p}{(2\pi)^3} E_q = -2N_f N_c \int \frac{d^4p}{(2\pi)^4} \ln(p_0^2 + E_q^2) + \mathrm{K}. \tag{13}$$

The infinite constant K is independent of the fermion mass, and hence it is dropped.

The dimensional regularization of Eq. (13) near three dimensions, $d = 3 - 2\epsilon$, leads to the potential up to zeroth order in ϵ as given by

$$\Omega_{q\bar{q}}^{\rm vac} = \frac{N_c N_f}{16\pi^2} m_q^4 \left\{ \frac{1}{\epsilon} - \frac{1}{2}\left[-3 + 2\gamma_E + 4\ln\left(\frac{m_q}{2\sqrt{\pi}M}\right)\right]\right\}, \tag{14}$$

where M denotes the arbitrary renormalization scale.

The addition of a counter term $\delta\mathcal{L}$ in the Lagrangian of the QM or PQM model,

$$\delta\mathcal{L} = \frac{N_c N_f}{16\pi^2} g^4\sigma^4 \left\{ \frac{1}{\epsilon} - \frac{1}{2}[-3 + 2\gamma_E - 4\ln(2\sqrt{\pi})]\right\}, \tag{15}$$

gives the renormalized fermion vacuum loop contribution as

$$\Omega_{q\bar{q}}^{\rm reg} = -\frac{N_c N_f}{8\pi^2} m_q^4 \ln\left(\frac{m_q}{M}\right). \tag{16}$$

The first term of Eq. (9), which is the vacuum contribution, will then be replaced by the appropriately renormalized fermion vacuum loop contribution as given in Eq. (16).

The relevant part of the effective potential in Eq. (8) that will fix the value of the parameters λ and v in the vacuum at $T = 0$ and $\mu = 0$ is the purely σ-dependent mesonic potential $U(\sigma)$ plus the renormalized vacuum term given by Eq. (16):

$$\begin{aligned}\Omega(\sigma) &= \Omega_{q\bar{q}}^{\rm reg} + U(\sigma) \\ &= -\frac{N_c N_f}{8\pi^2} g^4\sigma^4 \ln\left(\frac{g\sigma}{M}\right) - \frac{\lambda v^2}{2}\sigma^2 + \frac{\lambda}{4}\sigma^4 - h\sigma.\end{aligned} \tag{17}$$

The first derivative of $\Omega(\sigma)$ with respect to σ at $\sigma = f_\pi$ in the vacuum is set equal to zero:

$$\frac{\partial\Omega_{\rm MF}(0,0;\sigma,\Phi,\Phi^*)}{\partial\sigma} = \frac{\partial\Omega(\sigma)}{\partial\sigma} = 0. \tag{18}$$

The second derivative of $\Omega(\sigma)$ with respect to σ at $\sigma = f_\pi$ in the vacuum gives the mass of σ,

$$m_\sigma^2 = \frac{\partial^2\Omega_{\rm MF}(0,0;f_\pi,\Phi,\Phi^*)}{\partial\sigma^2} = \frac{\partial^2\Omega(\sigma)}{\partial\sigma^2}. \tag{19}$$

Solving Eqs. (18) and (19), we obtain

$$\lambda = \lambda_s + \frac{N_c N_f}{8\pi^2} g^4 \left[3 + 4\ln\left(\frac{g f_\pi}{M}\right)\right] \tag{20}$$

and

$$\lambda v^2 = (\lambda v^2)_s + \frac{N_c N_f}{4\pi^2} g^4 f_\pi^2, \tag{21}$$

where λ_s and $(\lambda v^2)_s$ are the values of the parameters in the pure sigma model:

$$\lambda_s = \frac{m_\sigma^2 - m_\pi^2}{2f_\pi^2}, \tag{22}$$

$$(\lambda v^2)_s = \frac{m_\sigma^2 - 3m_\pi^2}{2}. \tag{23}$$

It is evident from Eqs. (20) and (21) that the value of the parameters λ and v^2 have a logarithmic dependence on the arbitrary renormalization scale M. However, when we put the values of λ and λv^2 into Eq. (17), the M dependence cancels out neatly after the rearrangement of terms. Finally, we obtain

$$\Omega(\sigma) = -\frac{N_c N_f}{8\pi^2} g^4\sigma^4 \ln\left(\frac{\sigma}{f_\pi}\right) - \frac{\lambda_r v_r^2}{2}\sigma^2 + \frac{\lambda_r}{4}\sigma^4 - h\sigma. \tag{24}$$

Here, we define λ_r and $\lambda_r v_r^2$ as the values of the parameters after a proper accounting of the renormalized fermion vacuum contribution:

$$\lambda_r = \lambda_s + \frac{3N_c N_f}{8\pi^2} g^4 \tag{25}$$

and

$$\lambda_r v_r^2 = (\lambda v^2)_s + \frac{N_c N_f}{4\pi^2} g^4 f_\pi^2. \tag{26}$$

Now the thermodynamic grand potential for the PQM model in the presence of an appropriately renormalized fermionic vacuum contribution (PQMVT model) will be written as

$$\begin{aligned}\Omega_{\rm MF}(T,\mu;\sigma,\Phi,\Phi^*) = \mathcal{U}(T;\Phi,\Phi^*) + \Omega(\sigma) \\ + \Omega_{q\bar{q}}^{\rm T}(T,\mu;\sigma,\Phi,\Phi^*).\end{aligned} \tag{27}$$

Thus in the PQMVT model one can get the chiral condensate σ and the Polyakov loop expectation values Φ, Φ^* by searching the global minima of the grand potential in Eq. (27) for a given value of temperature T and chemical potential μ:

$$\frac{\partial\Omega_{\rm MF}}{\partial\sigma} = \frac{\partial\Omega_{\rm MF}}{\partial\Phi} = \frac{\partial\Omega_{\rm MF}}{\partial\Phi^*} = 0. \tag{28}$$

We will take the values $m_\pi = 138$ MeV, $m_\sigma = 500$ MeV, and $f_\pi = 93$ MeV in our numerical computation. The constituent quark mass in vacuum $m_q^0 = 310$ MeV fixes the value of the Yukawa coupling $g = 3.3$.

III. THE PROXIMITY OF THE TCP TO THE CEP AND THE PHASE STRUCTURE

In the phase diagram of two quark flavor massless QCD [20], the second-order line of O(4) critical points starts from the temperature axis at $\mu = 0$ in the μ and T plane and terminates at the tricritical point. Here it happens to meet the first-order transition line coming from the lowest temperature on the μ axis. For broken-chiral-symmetry QCD with two light quarks, the TCP disappears from the phase diagram because the transition on the temperature axis at $\mu = 0$ becomes a crossover. Further, the line of

crossover transition points joins the first-order transition line in the phase diagram at the critical end point where the phase transition turns second-order. The two-flavor QMVT and PQMVT models have become QCD-like effective models due to the proper accounting of the fermionic vacuum fluctuation. Hence one must find a TCP in the μ and T plane of the phase diagram computed in the chiral limit of zero pion mass. In the present work, we compute the phase diagram for $m_\pi = 138$ MeV and locate the CEP in the μ and T plane of all four models: QMVT, PQMVT, QM, and PQM. Next, we locate the TCP in our calculation and quantify its proximity to the CEP. The presence of the TCP in a model and its distance from the CEP in the phase diagram influences the nature of criticality around the CEP.

We present the QMVT and PQMVT model phase diagrams in Fig. 1(a), computed with $m_\pi = 138$ MeV and $m_\pi = 0$ MeV. Figure 1(b) describes the QM and PQM model phase diagrams for $m_\pi = 138$ MeV. Solid lines denoting the first-order chiral phase transition in Fig. 1 merge with the small dashed (green) lines representing the chiral crossover at the CEP (shown by filled circles) for $m_\pi = 138$ MeV computations. The ± 5 MeV error bars (in a range $\mu = 100$ to $\mu = 160$ MeV) on the small dashed line in the upper half of Fig. 1(a) signify the ambiguity of pseudocritical temperature determination for the chiral crossover in the PQMVT model calculations (see Ref. [98] for details). The solid lines (magenta in color) around the CEP are the contours of constant ratio ($R_q = 2$) of quark number susceptibility obtained in a model and the quark number susceptibility value for a free quark gas. Since quark number susceptibility diverges at the CEP such contours signify the extent of critical fluctuations around the CEP. The CEP in the QMVT model at $\mu_{\rm CEP} = 299.35$ MeV and $T_{\rm CEP} = 32.24$ MeV in the lower half of Fig. 1(a) shifts to the higher value on the temperature axis at $T_{\rm CEP} = 83.0$ MeV and $\mu_{\rm CEP} = 295.217$ MeV in the PQMVT model. Similarly, the QM model CEP at $T_{\rm CEP} = 102.09$ MeV and $\mu_{\rm CEP} = 151.7$ MeV shifts towards the temperature axis at $T_{\rm CEP} = 166.88$ MeV and $\mu_{\rm CEP} = 81.02$ MeV in the upper half of Fig. 1(b) due to the influence of the Polyakov loop potential. Comparing the CEP position in the QM and PQM models in Fig. 1(b), respectively, to the location of the CEP in the QMVT and PQMVT models in Fig. 1(a) we find a considerably significant shift of the CEP to larger chemical potential and smaller temperature values for the QMVT and PQMVT models due to the very robust influence of the fermionic vacuum term in the effective potential. The first-order phase transition becomes stronger in the influence of Ployakov loop potential. However, its strength becomes so weak due to the strong effect of the fermionic vacuum correction that the length of the first-order line decreases significantly and we find a strong shrinkage of the phase coexistence region in the PQMVT model phase diagram. These results extend our recently reported work [98] and facilitate the details of model comparison for the two-quark-flavor case. Further, these results are also in qualitative agreement with the recent results of Schaefer *et al.* [99] for the 2 + 1-flavor case.

The temperature for the chiral crossover transition at $\mu = 0$ is highest in the PQMVT model phase diagram in Fig. 1(a) due to the combined effect of the Polyakov loop potential and the fermionic vacuum correction. The effect of only the fermionic vacuum correction is seen in the

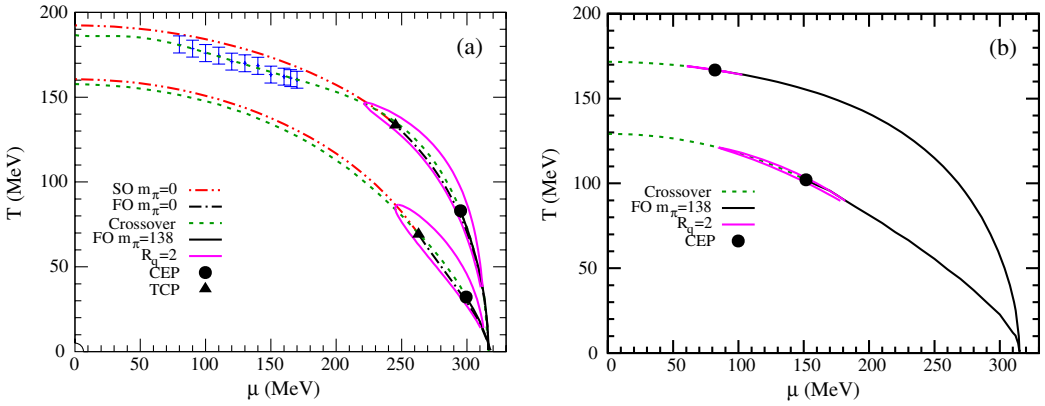

FIG. 1 (color online). (a) For calculations with an experimental pion mass, solid lines representing the first-order (FO) chiral phase transition merge with the small dashed lines (green in color) for the chiral crossover at the CEP, which is denoted by the filled circle. The solid lines (magenta in color) around the CEP are the contours of constant normalized quark number susceptibility $R_q = 2$. For calculations with zero pion mass, dash dot lines represent the first-order phase transition in the chiral limit of the QMVT and PQMVT models, while the dash double dot lines denote the second-order (SO) transition, and the filled triangle is the location of the TCP where these two lines merge into each other. The lower part of the figure shows the QMVT model results while the upper part shows the PQMVT results. (b) The lower half of the figure shows the QM model results while the upper half shows the PQM results. The line types represent the same data as in Fig. 1(a) for calculations with experimental pion mass.

higher value of the temperature for the $\mu = 0$ chiral crossover in the QMVT model if we compare the lower halves of Figs. 1(a) and 1(b) for the respective phase diagrams of the QMVT and QM models. It will be interesting to compare our QMVT/PQMVT model findings with the NJL/PNJL model results because these calculations explicitly include the fermion vacuum loop contribution up to an ultraviolet cutoff Λ. Scavenius *et al.* [45] compared the two-flavor sigma model and the NJL model calculations and concluded that the energy difference (effective bag constant) between the global minimum and the local maximum of the effective potential in vacuum is responsible for the difference in the temperatures corresponding to the crossover transition at $\mu = 0$, which is about 140 MeV in the sigma model and about 180–190 MeV in the NJL model. This difference is largely due to the absence of a logarithmic fermionic vacuum correction in the sigma model. The $\mu = 0$ crossover transition temperature is about 225 (280) MeV in the NJL (PNJL) model computation by Costa *et al.* [92]. This temperature is reduced in a recent nonlocal PNJL model computation by Contrera *et al.* [93]; still, it is found in a range of 209–215 MeV for different sets of parametrizations. In a very recent beyond-mean-field nonlocal PNJL model computation [75], there was an indication of a further decrease in the temperature of the crossover transition at $\mu = 0$. Here, with the proper accounting of the logarithmic correction in our extended σ model computations, the crossover at $\mu = 0$ occurs at a temperature of about 187 (158) MeV in the PQMVT (QMVT) model, registering an increase of about 15–28 MeV over the corresponding crossover temperature of about 172 (130) MeV in the PQM (QM) model. We notice that different values of the crossover temperature at $\mu = 0$ give rise to the different locations of the CEP. The PNJL (NJL) model computation in Ref. [92] locates the CEP at $T_{\mathrm{CEP}} = 169.11(79.92)$ MeV and $\mu_{\mathrm{CEP}} = 321.32(331.72)$ MeV, while it is found at a significantly smaller temperature of $T_{\mathrm{CEP}} = 83(32.24)$ MeV and $\mu_{\mathrm{CEP}} = 295.22(299.35)$ MeV in our PQMVT (QMVT) model computation.

We recall that, contrary to the sigma model, the NJL model is a nonrenormalizable theory which is usually regularized by a noncovariant ultraviolet cutoff Λ. One should take the quantitative predictions of the NJL/PNJL model with care because in order to generate phase diagrams similar to the linear sigma model one requires very high values of G, which in turn generates high effective quark masses at zero μ and T. Even when the value of the effective quark mass generated by those parameters becomes larger than Λ, the values of relevant observables—such as the quark condensate and the pion decay constant—remain well within reasonable values [30]. In the extended sigma model computations as well the value of the $\mu = 0$ crossover temperature, the structure of the phase diagram, and the position of the CEP (and of the TCP in the chiral limit) are quite sensitive to different parametrizations and approximations. Larger value of m_σ in general pushes the CEP towards the μ axis, and for $m_\sigma = 600$ MeV in the PQMVT model computation [98,99] the CEP disappears from the phase diagram.

Here it is relevant to point out that the mesonic sector contributes only at the tree level in our present work, and the bosonic thermal and vacuum fluctuations are not included. A recent investigation of the chiral dynamics of two-flavor QCD by Andersen *et al.* [47] reports that the properties of the phase transition—the order and the critical temperature—depend crucially on the approximations made, i.e., whether or not one includes the bosonic and fermionic vacuum fluctuations in the effective potential. They included all contributions (vacuum as well as thermal) from both fermions and bosons in their full one-loop calculation in an optimized perturbation theory framework and found that the CEP disappears from the phase diagram for a physical pion mass, and the transition becomes a crossover in the entire μ and T plane. It has also been reported that for small values of the vacuum pion mass (50 MeV) the phase diagram of the linear sigma model [29] has two distinct first-order lines terminating in two critical points. This behavior is caused by the thermal fluctuations of the mesonic fields, which are incorporated by adopting a self-consistent method [49]. Very recently, Ferroni and Koch [30] found the appearance of multiple critical points in their extensive thermodynamical analysis considering beyond-mean-field thermal fluctuations.

In the chiral limit of the QMVT and PQMVT model computations with zero pion mass, the dash dot lines denoting a first-order phase transition in Fig. 1(a) merge with the dash double dot lines representing the second-order transition at the TCP (shown by the filled triangle). Again, due to the influence of the Polyakov loop potential, the QMVT model TCP at $T_t = 69.06$ MeV and $\mu_t = 263.0$ MeV in the lower half of Fig. 1(a) shifts to its upper half at $T_t = 133.5$ MeV and $\mu_t = 245.34$ MeV for the PQMVT model. We quantified the proximity of the TCP to the CEP in the phase diagram by plotting the constant normalized quark number susceptibility ($R_q = 2$) contour around the CEP. This contour is quite large in both directions; the chemical potential as well as the temperature. The TCP position is well inside this contour on the phase diagram. It means that the shape of the critical region and the nature of criticality around the CEP becomes significantly influenced by the presence of the TCP in the corresponding chiral limit. This is also corroborated by our calculation of critical exponents that we present in the next section. The TCP does not exist in the phase diagram of the QM and PQM models because the phase transition at $\mu = 0$ on the temperature axis is of first order in the chiral limit of zero pion mass. Costa *et al.* [92] also located the TCP in the chiral limit of the NJL/PNJL model calculation and found that the TCP lies just on the periphery of the

$R_q = 2$ contour around the CEP. They further found that the TCP does not have a qualitative effect on the criticality around the CEP and critical exponents calculated from the divergence of the quark number susceptibility near the CEP are mostly found to have a mean-field value of $.66 \pm .01$: the critical exponent becomes $.69 \pm .02$ in the PNJL model when $\mu_{\rm CEP}$ is approached from the higher μ side at constant $T = T_{\rm CEP}$. The TCP was also located in a nonlocal PNJL model computation in Ref. [93] where it was concluded that the position of the TCP does not influence the critical behavior around the CEP.

A. Susceptibility contours and criticality

We require the quantification of criticality around the CEP for the experimental finding of the CEP in relativistic heavy ion collisions. The crossover transition is marked by a peak in the quark number susceptibility which becomes sharper and higher as one approaches the CEP in the phase diagram from the crossover side, and finally the peak diverges at the CEP. Hence the quark number susceptibilities and scalar susceptibilities will be significantly enhanced in a region around the CEP in the μ and T plane in comparison to their respective values for the free quark gas. Thus the contour regions of properly normalized constant quark number susceptibilities and scalar susceptibilities can be taken as the measure of criticality around the CEP. The ratio of the quark number susceptibility χ_q normalized to the free susceptibility $\chi_q^{\rm free}$ is written as

$$R_q = \frac{\chi_q}{\chi_q^{\rm free}}. \tag{29}$$

The expression of the quark number susceptibility is obtained as

$$\chi_q = -\frac{\partial^2 \Omega_{\rm MF}}{\partial \mu^2}, \tag{30}$$

$$\lim_{m_q \to 0} \chi_q(T,\mu) = \frac{\nu_q}{6}\left[T^2 + \frac{3\mu^2}{\pi^2}\right] \equiv \chi_q^{\rm free}, \tag{31}$$

$$\nu_q = 2N_c N_f = 12. \tag{32}$$

The first and second partial derivatives of the σ, Φ, and Φ^* fields with respect to chemical potential contribute in the double derivatives of $\Omega(\sigma)$, $\mathcal{U}_{\rm log}$, and $\Omega_{q\bar{q}}^{\rm T}$ with respect to the chemical potential as given in Appendix A of Ref. [98].

In Fig. 2 we have plotted contours for three constant ratios $R_q = 2$, 3, and 5 in the μ and T plane relative to the CEP. If we compare the contours depicting the PQM model results in Fig. 2(a) to the contours showing the pure QM model results in Fig. 2(b), we conclude that the presence of the Polyakov loop potential compresses the critical region, particularly in the T direction, similar to the findings of Schaefer *et al.* [99] in their 2 + 1-quark-flavor calculation. The compression of the critical region in the T direction is much more pronounced in our two-quark-flavor calculation, as can be seen in the spread of the $R_q = 2$ contour on the temperature axis in only a small range of ± 2.5 MeV near $T_{\rm CEP}$. The modification in the μ direction is moderate compared to the effect in the T direction. Since the chiral crossover transition becomes faster and sharper due to the Polyakov loop contribution in the effective potential, the critical region in the T direction becomes significantly compressed.

The contours in Fig. 3 are the signatures of a significantly robust influence of the fermionic vacuum fluctuations on the size and shape of the critical region. The size of the critical region is increased in a direction perpendicular to the crossover line due to the effect of the fermionic vacuum fluctuations. This effect is less pronounced in Fig. 3(a) due to the compression of the critical region width because of the presence of the Polyakov loop potential contribution in the PQMVT model, while the QMVT model results of Fig. 3(b) obtained in the absence of the Polyakov loop show a robust increase in the width of the critical region. However, the extent and size of the critical region in the PQMVT model in Fig. 3(a) is noticeably

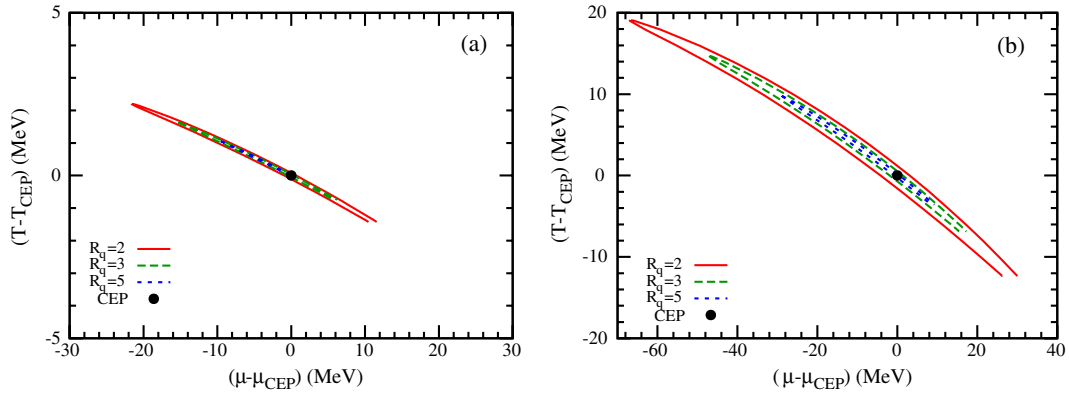

FIG. 2 (color online). (a) The contours of three different values for the constant ratios $R_q = 2$, 3, and 5 of quark number susceptibility to the quark susceptibility for the free quark gas are plotted in the PQM model calculations. (b) Similar contours are plotted in the QM model computations.

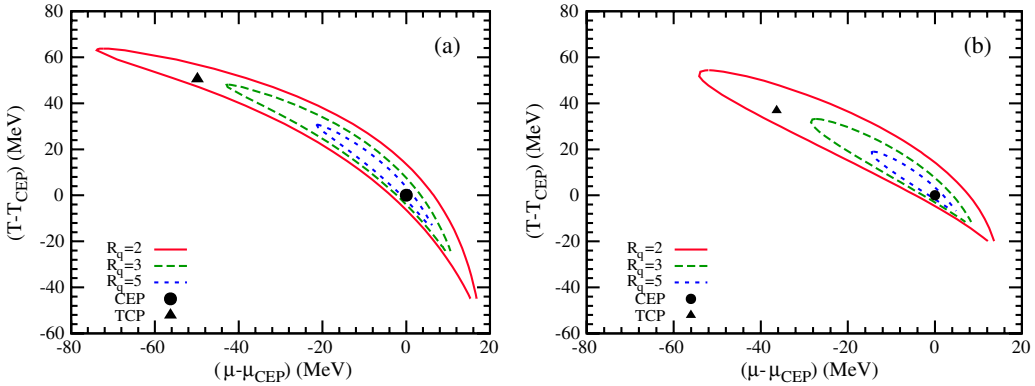

FIG. 3 (color online). (a) The contours of three different values for the constant ratios $R_q = 2$, 3, and 5 of quark number susceptibility to the quark susceptibility for the free quark gas are plotted in the PQMVT model calculations. (b) Similar contours are plotted in the QMVT model calculations.

larger in both the μ and T directions when compared with the QMVT model's region of criticality in Fig. 3(b). Fermionic vacuum fluctuations push the CEP to larger chemical potentials in both the QMVT and PQMVT models. Since the quark determinant gets modified mostly at moderate chemical potentials by the Polyakov loop potential and the PQMVT model CEP shifts to a higher critical temperature [cf. also Fig. 1] and lower chemical potential when compared to the CEP in the QMVT model, we obtain an enhancement of the critical region in the PQMVT model. Further, the chiral crossover transition becomes much smoother because the phase transitions in general get washed out by the influence of fluctuations. This leads to a critical region which is broader in the direction perpendicular to the extended first-order transition line. The size of the critical region for $(\mu\text{-}\mu_{\rm CEP}) > 0$ is comparable in both the QMVT and PQMVT models because the influence of the Polyakov loop potential becomes insignificant for smaller temperatures and larger chemical potentials. In Fig. 3, filled circles show the position of the CEP and the filled triangles show the location of the TCP. We observe that the TCP is located outside the $R_q = 3$ contour but well inside the $R_q = 2$ contour for both the QMVT and PQMVT models.

If we compare our two-quark-flavor results with the 2 + 1-flavor calculations in the renormalized PQM/QM models in Ref. [99], we notice that in the absence of strange quarks the effect of the fermionic vacuum term leads to an enhanced critical region in both the T and μ directions, and that the size of the contours is larger in our two-flavor calculation. We point out that the 2 + 1-flavor calculation in Ref. [99] was done with $m_\sigma = 400$ MeV and $T_0 = 270$ MeV, while in our two-flavor calculation $m_\sigma = 500$ MeV and $T_0 = 208$ MeV. In general, a higher value of m_σ pushes the CEP to a higher chemical potential. In our two quark flavor calculation, the CEP is at $(T_{\rm CEP}, \mu_{\rm CEP}) = (83.0, 295.217)$ MeV and (32.24, 299.35) MeV, respectively, in the PQMVT and QMVT model computations, while the CEP in the corresponding 2 + 1-flavor model computation of Ref. [99] is at $(T_{\rm CEP}, \mu_{\rm CEP}) = (90.0, 283.0)$ MeV and (32, 286) MeV.

The zero-momentum projection of the scalar propagator encodes all fluctuations of the order parameter, and it corresponds to the scalar susceptibility χ_σ. The relation of the scalar susceptibility to the order parameter is obtained as [24,25,51,91]

$$\chi_\sigma = -\frac{\partial^2 \Omega_{\rm MF}}{\partial h^2}. \tag{33}$$

The most rapid change of the chiral order parameter should be coincident with the maximum in the temperature or quark chemical potential variation of χ_σ. The relation of the scalar susceptibility to the sigma mass via $\chi_\sigma \sim m_\sigma^{-2}$ can be easily verified. The normalized scalar susceptibility is written as [51]

$$R_s(T, \mu) = \frac{\chi_\sigma(T, \mu)}{\chi_\sigma(0, 0)}. \tag{34}$$

In Fig. 4 we plot the contours for three values of fixed ratios R_s around the CEP in the PQM and QM models. The $R_s = 10$ contour in Fig. 4(a) is compressed in the T direction, and its extension in the μ direction is also reduced in comparison to the pure QM model contours in Fig. 4(b). This is due to the quite rapid temperature or chemical potential variation of the σ meson mass m_σ on account of the faster and sharper change of the order parameter for the chiral crossover in the presence of the Polyakov loop potential. We do not find a contour for $R_s = 25$ in Fig. 4(a) because the minimum value of the σ meson mass does not fall below 100 MeV, though the value of m_σ falls very rapidly from 500 MeV to 128 MeV, giving rise to a very thin and small contour region even for $R_s = 15$. In the QM model computations, we get all of the contour regions for $R_s = 10$, 15, and 25 with well-defined sizes because the m_σ variation is smoother and slower in comparison to the corresponding PQM model results, and further the minimum in the m_σ variation at the CEP approaches a value of almost zero. The chiral crossover transition on the temperature axis at $\mu = 0$ MeV in the QM and PQM models is

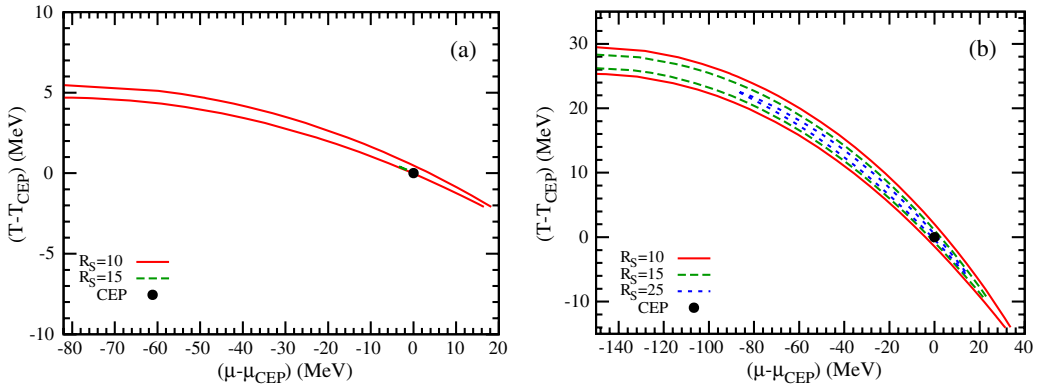

FIG. 4 (color online). (a) The contours of different values for the constant ratios $R_S = 10$ and 15 of T- and μ-dependent scalar susceptibility to the scalar susceptibility at $T = 0$ and $\mu = 0$ MeV are plotted in the PQM model computations. (b) Similar contours for the constant ratios $R_S = 10$, 15, and 25 are plotted in the QM model computations.

quite sharp and fast because it emerges from the background of a first-order chiral transition at $\mu = 0$ MeV in the corresponding chiral limit of zero pion mass, and we do not find the existence of a TCP in the QM and PQM models. As a consequence, we do not find the closure of the $R_s = 10$ contour on the temperature axis at $\mu = 0$ MeV.

We obtain quite well-defined and closed contour regions for $R_s = 10$, 15, and 25 in Fig. 5, which again become broader in the direction perpendicular to the crossover line due to the effect of the fermionic vacuum fluctuations in the QMVT and PQMVT model calculations. In addition, the critical region for the scalar susceptibility is elongated in the phase diagram and χ_σ is enhanced in the direction parallel to the first-order transition line. Here also the presence of the Polyakov loop potential in the PQMVT model leads to the compression in the width of the critical region around the CEP, as shown in Fig. 5(a). The fermionic vacuum fluctuations make the chiral crossover transition very smooth, while the Polyakov loop potential makes it sharper and faster, and these opposite effects give a typical shape to the quark number susceptibility contours in Fig. 3(a) in the PQMVT model. Similar effects are seen in the scalar susceptibility contours in Fig. 5(a). The χ_σ contours in Fig. 5(b) for the QMVT model are broader and rounded due only to the effect of the fermionic vacuum fluctuations.

To obtain a detailed understanding and analysis of the criticality around the CEP we will be studying the critical exponents of the susceptibilities at the critical point in the next section.

B. Critical exponents

The quark number susceptibility peak signifying the crossover transition diverges at the CEP when it is approached from the crossover side of the phase diagram. This divergence is governed by a power law within the critical region. The corresponding critical exponents depend on the route through which the singularity (CEP) is approached in the μ and T plane [102]. This path dependence decides the shape of the critical region. In the mean-field approximation, the quark number susceptibility scales with an exponent $\gamma_q = 1$ for a path

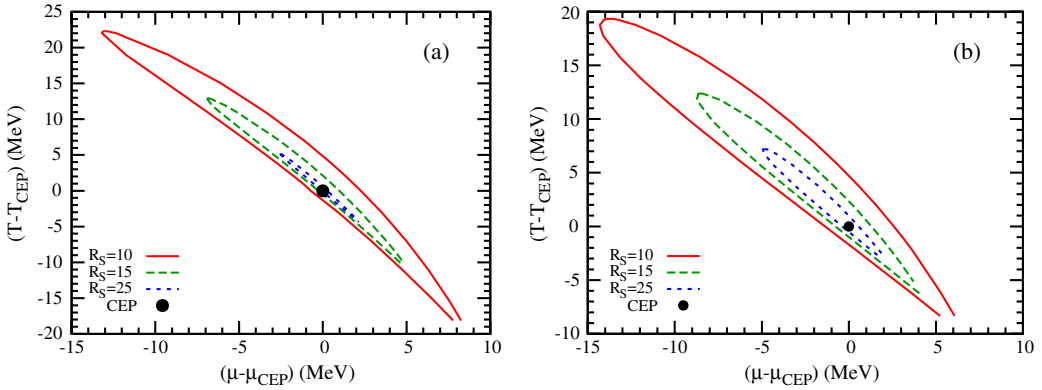

FIG. 5 (color online). (a) The contours of three different values for the constant ratios $R_S = 10$, 15, and 25 of T- and μ-dependent scalar susceptibility to the scalar susceptibility at $T = 0$ and $\mu = 0$ MeV are plotted in the PQMVT model computations. (b) Similar contours for the constant ratios $R_S = 10$, 15, and 25 are plotted in the QMVT model calculations.

asymptotically parallel to the first-order transition line, and for any other path which is not parallel to the first-order line the divergence scales with the exponent $\epsilon = 2/3$. This larger critical exponent ($\gamma_q > \epsilon$) is an important reason for the elongation of the critical region in a direction parallel to the first-order line, as already pointed out in Refs. [24,51].

In order to further investigate the nature of criticality in two quark flavor computations, we have numerically evaluated the critical exponents of the quark number susceptibility χ_q in the QM, PQM, QMVT, and PQMVT models. In these investigations, the critical $\mu_{\rm CEP}$ at a fixed critical temperature $T_{\rm CEP}$ is approached from the lower- as well as higher-μ sides in a path parallel to the μ axis in the (T, μ) plane. The calculation of the critical exponents has been done with the following linear logarithmic fit formula:

$$\log\chi_q = -m\log|\mu\text{-}\mu_{\rm CEP}| + c. \tag{35}$$

The slope m gives the critical exponent ϵ and the y axis intercept c is independent of μ. Figure 6 shows the logarithm of χ_q as a function of the logarithm of $(\mu\text{-}\mu_{\rm CEP})$ close to the CEP in the QM model. Scaling is observed over several orders of magnitude. In Fig. 6(a) the $\mu_{\rm CEP}$ is approached from the lower-μ side and we obtain a critical exponent $\epsilon = m = 0.6379 \pm 0.0002$, while the critical exponent $\epsilon = m = 0.6648 \pm 0.0001$ in the result of Fig. 6(b) when the $\mu_{\rm CEP}$ is approached from the higher-μ side. The scaling starts around around $\log|\mu\text{-}\mu_{\rm CEP}| < -.5$ in both cases. These exponents show good agreement with the mean-field prediction $\epsilon = 2/3$. In Fig. 6(a) the data fitted in the range $1.0 < \log|\mu\text{-}\mu_{\rm CEP}| < 2.0$ also shows a type of scaling linear behavior over one order of magnitude with a larger slope $n = .6807 \pm .0002$, which changes to $m = .6379 \pm .0002$ in the range $-.5 < \log|\mu\text{-}\mu_{\rm CEP}| < 1.0$. When $\log|\mu\text{-}\mu_{\rm CEP}| \sim 2.0$, we are very close to $\mu = 0$ on the temperature axis. The phase transition at $\mu = 0$ is of first order for the chiral limit ($m_\pi = 0$) in the QM model, and it becomes a crossover for the actual pion mass. In the quark mass (or the pion mass) and T plane at $\mu = 0$, the first-order transition line should change to a crossover line through another second-order critical end point as we increase the pion mass from zero to the experimental value. This linear behavior in a range $1.0 < \log|\mu\text{-}\mu_{\rm CEP}| < 2.0$ with a larger slope seems to be the consequence of another hidden CEP in the mass and temperature plane at $\mu = 0$ in the QM model. The critical exponent values obtained in the PQM model computation have been given in Table I. We can see that the presence of the Polyakov loop potential in the QM model does not influence the value of the critical exponents. Figure 7 shows the plot of the logarithm of χ_q with respect to the logarithm of $(\mu\text{-}\mu_{\rm CEP})$ in the presence of the fermionic vacuum fluctuations in the QMVT model. In Fig. 7(a), if we approach the $\mu_{\rm CEP}$ from the lower-μ side, we obtain a critical exponent $\epsilon = m = 0.720 \pm 0.00005$, which is larger than the QM model result. This larger critical exponent seems to be the consequence of the modification of criticality around the CEP due to the proximity of the TCP. The TCP in the QMVT model computation (with $m_\pi = 0$) owes its existence to the influence of the fermionic vacuum fluctuation, and it lies quite well within the $R_q = 2$ contour surrounding the CEP in the phase diagram in Fig. 1(a). We observe a scaling over several orders of magnitude, and it

TABLE I. Critical exponents of the quark number susceptibility in the QM, PQM, QMVT, and PQMVT models for two different paths parallel to the chemical potential axis approaching the $\mu_{\rm CEP}$ from the lower $\mu < \mu_{\rm CEP}$ and higher $\mu > \mu_{\rm CEP}$ side.

Model	$\mu\text{-}\mu_{\rm CEP} < 0$	$\mu\text{-}\mu_{\rm CEP} > 0$
QM	0.6379 ± 0.0002	0.6648 ± 0.0001
PQM	0.6309 ± 0.0001	0.6668 ± 0.0001
QMVT	0.720 ± 0.00005	0.6938 ± 0.0002
PQMVT	0.725 ± 0.0002	0.6886 ± 0.0004

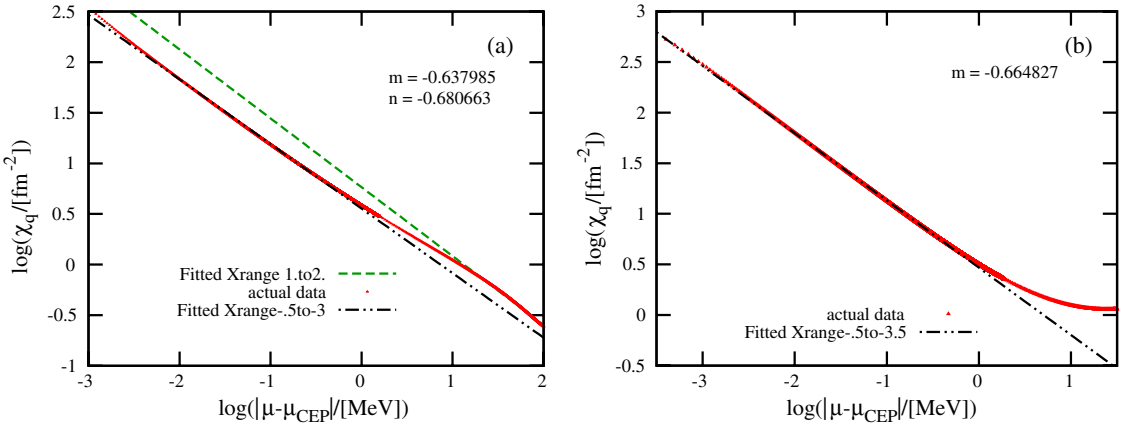

FIG. 6 (color online). (a) The plot of the logarithm of χ_q as a function of the logarithm of $(\mu\text{-}\mu_{\rm CEP})$ close to the CEP in the QM model when the $\mu_{\rm CEP}$ is approached from the lower-μ side. (b) The same plot as in Fig. 6(a) in the QM model when the $\mu_{\rm CEP}$ is approached from the higher-μ side.

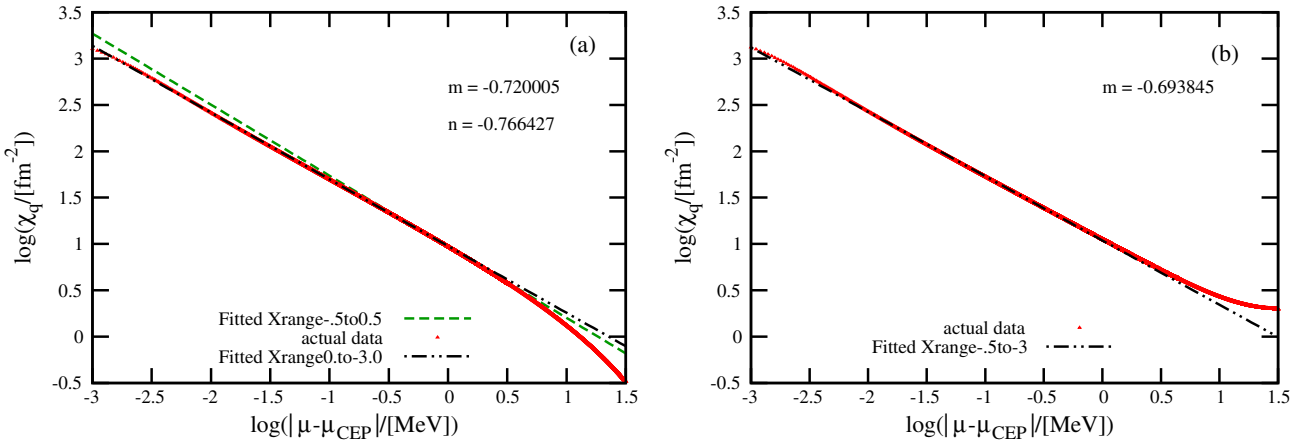

FIG. 7 (color online). (a) Plot of the logarithm of χ_q as a function of the logarithm of $(\mu\text{-}\mu_{\mathrm{CEP}})$ close to the CEP in the QMVT model when the μ_{CEP} is approached from the lower-μ side (b) The same plot as in Fig. 7(a) in the QMVT model when the μ_{CEP} is approached from the higher-μ side.

starts earlier when $\log|\mu\text{-}\mu_{\mathrm{CEP}}| < 0.0$. This higher value of the critical exponent is close to the value calculated in Ref. [51] where the effect of quantum fluctuations in the QM model were incorporated in the proper-time renormalization group approach. The critical exponents change in the range $-0.5 < \log|\mu\text{-}\mu_{\mathrm{CEP}}| < .5$ in Ref. [51], from .77 for the scaling regime starting after $\log|\mu\text{-}\mu_{\mathrm{CEP}}| > .5$, to .74 for another scaling regime starting before $\log|\mu\text{-}\mu_{\mathrm{CEP}}| < -.5$. Though we do not find analogous crossing behavior of the universality classes, the data points in our calculation show a bending trend, and when we fit the data in a small range, $-0.5 < \log|\mu\text{-}\mu_{\mathrm{CEP}}| < .5$, we find a higher slope $\epsilon = m = 0.7664 \pm 0.0002$, as shown in the Fig. 7(a). In our calculation, the critical region of the CEP is having a noticeable overlap with the critical region of the TCP and this seems to be the reason of the bending trend noticed in the data. If we approach the CEP from the higher-μ side, we find a smaller critical exponent $\epsilon = m = 0.6938 \pm 0.0002$ in the result of Fig. 7(b). In this case, the scaling starts around $\log|\mu\text{-}\mu_{\mathrm{CEP}}| < -.5$. We point out that these exponents computed in the presence of the fermionic vacuum term in the QM model are different from the mean-field prediction $\epsilon = 2/3$. Similar results are found in Fig. 8, which shows the plot of the logarithm of χ_q with respect to the logarithm of $(\mu\text{-}\mu_{\mathrm{CEP}})$ in the presence of the fermionic vacuum fluctuation in the PQMVT model. The presence of the Polyakov loop compresses the width of the critical region in the PQMVT model, but its effect on critical exponents is negligibly small, as can be seen in Figs. 8(a) and 8(b). Here we mention that the recent $2+1$-flavor model calculation in Ref. [99] does not report any modification of the mean-field critical exponents due to the influence of the fermionic vacuum term. It is well-known that the chiral transition on the temperature axis at $\mu = 0$ for the two flavors of massless quarks changes from the second to the

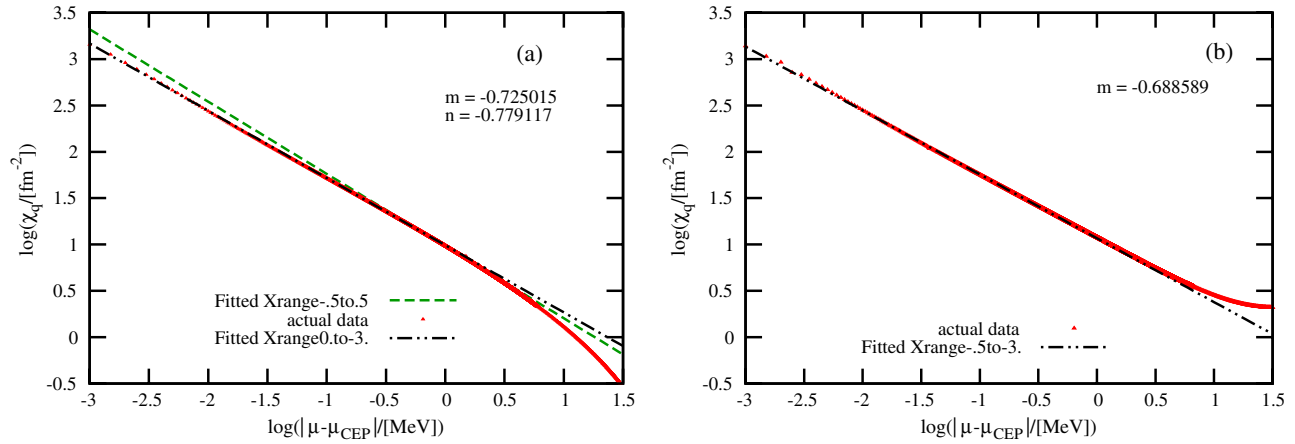

FIG. 8 (color online). (a) Plot of the logarithm of χ_q as a function of the logarithm of $(\mu\text{-}\mu_{\mathrm{CEP}})$ close to the CEP in the PQMVT model when the μ_{CEP} is approached from the lower μ side (b) The same plot as in Fig. 8(a) in the PQMVT model when the μ_{CEP} is approached from the higher-μ side.

first order in the presence of a third massless quark, i.e., the s quark [20]. Further, the precise location of the CEP in the 2 + 1-flavor calculation is also quite sensitive to the mass of the s quark [92]. Even though the fermionic vacuum fluctuation makes the chiral transition smoother and weaker, its effect on the power-law divergence of χ_q in the vicinity of the CEP seems to be offset by the presence of the physical s quark in the 2 + 1-flavor calculation in Ref. [99]. The critical exponents calculated in all the models are summarized and tabulated in Table I.

C. In medium meson masses

The critical fluctuations are also encoded in the variation of meson masses $m_\pi(T, \mu)$ and $m_\sigma(T, \mu)$ as one passes through the chiral-symmetry-restoring phase transition. We will investigate and compare the "in-medium" meson mass variations in the QM, QMVT, PQM, and PQMVT models in order to see the influence of the fermionic vacuum fluctuations. The sigma and pion masses are calculated by determining the curvature of the grand potential at the global minimum:

$$m^2_{\pi,i}(T, \mu) = \frac{\partial^2 \Omega(T, \mu)}{\partial \pi_i \partial \pi_i}\Bigg|_{\min}, \tag{36}$$

$$m^2_{\sigma}(T, \mu) = \frac{\partial^2 \Omega(T, \mu)}{\partial \sigma \partial \sigma}\Bigg|_{\min}. \tag{37}$$

The left panel of Fig. 9 shows the temperature variations of meson masses for $\mu = 0$, $\mu = \mu_{\rm CEP}$, and $\mu > \mu_{\rm CEP}$ in the QM model, while the right panel shows the corresponding variations in the QMVT model. In the chiral-symmetry-broken mesonic phase, the sigma mass always decreases with temperature. The sigma mass increases again at high temperatures, signaling chiral-symmetry restoration, and it becomes degenerate with increasing pion mass, which does not vary much below the transition temperature. The degenerate meson masses increase linearly with T after the chiral-symmetry restoration transition [51] has taken place. The temperature variations of the m_σ and m_π masses at $\mu = 0$ in Fig. 9(b) are significantly modified due to the presence of fermionic vacuum fluctuations in the QMVT model. If we compare these variations with the corresponding QM model temperature variations of masses in Fig. 9(a), we find that the mass degeneration in m_σ and m_π at $\mu = 0$ in Fig. 9(b) becomes very smooth, and it takes place at a higher temperature. Since the chiral crossover on the temperature axis at $\mu = 0$ is quite sharp and fast in the QM model, the mass degeneration trend in the m_σ and m_π is also quite sharp and fast in Fig. 9(a). Fermionic vacuum fluctuations make the chiral crossover at $\mu = 0$ very smooth in the QMVT model, and this is also reflected in the setting up of a very smooth mass degeneration trend at $\mu = 0$ in Fig. 9(b). Long-wavelength fluctuations of the order parameter characterize the second-order phase transitions. Since the chiral phase transition turns second-order at the CEP, the sigma meson mass must vanish at the CEP because the effective potential completely flattens in the radial direction. Thus the sigma meson mass drops below the pion mass near the CEP and it becomes almost zero at $\mu_{\rm CEP} = 299.35$ MeV in the QMVT model, as shown in Fig. 9(b). The sigma mass goes to zero only at $\mu_{\rm CEP} = 151.7$ MeV in Fig. 9(a) in the QM model. The discontinuities in mass evolutions, respectively, in Figs. 9(a) and 9(b), signal a first-order phase transition at small temperatures when $\mu > \mu_{\rm CEP} = 305$ MeV in both the QM and QMVT models.

Here it is worthwhile to mention that the calculation of the sigma and pion masses in the NJL model is not as straightforward as in the linear sigma model because the σ

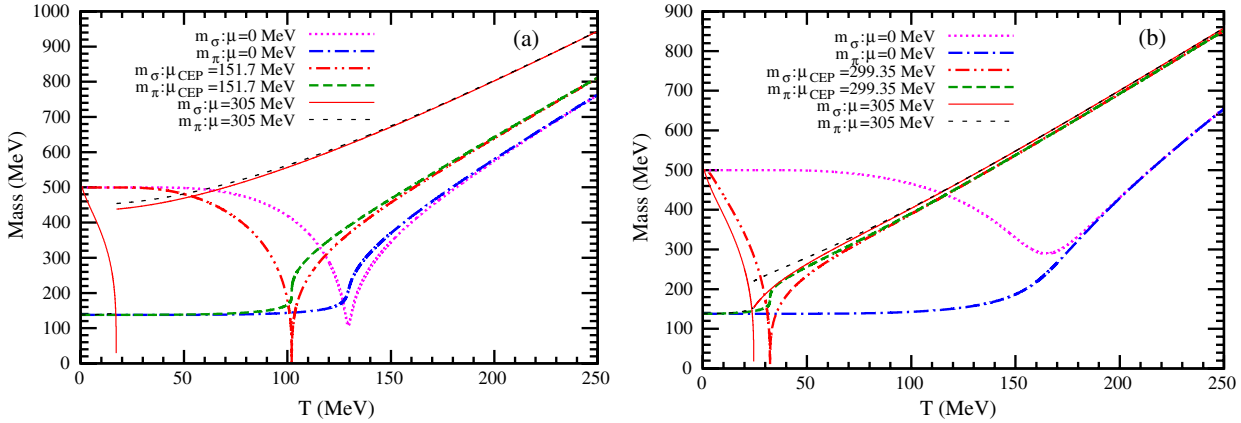

FIG. 9 (color online). (a) Temperature variations of meson masses in the QM model. The dotted line and the dash dot line in the rightmost part of the figure represent the temperature variations of m_σ and m_π, respectively, at $\mu = 0$, the dashed line with two dots in the middle part represents m_σ, and the line with the small dash represents the m_π temperature variation at $\mu_{\rm CEP} = 151.7$ MeV; the solid line in the leftmost part of the figure represents m_σ while the line with the thinner dash denotes the m_π temperature variation at $\mu = 305$ MeV. (b) Temperature variations of m_σ and m_π under the influence of fermionic vacuum fluctuations for the QMVT model computations. Lines represent the same mass variations as in the left panel of the figure. In the QMVT model, $\mu_{\rm CEP} = 299.35$ MeV.

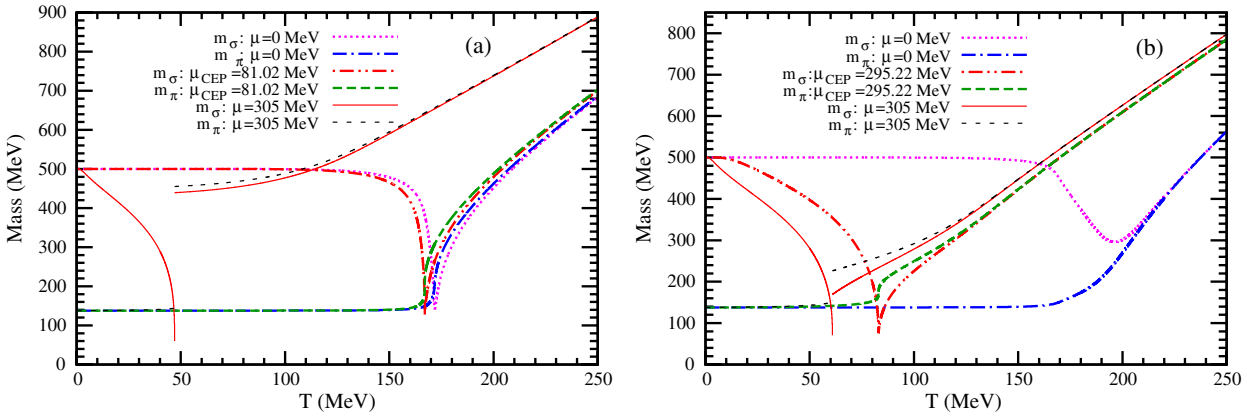

FIG. 10 (color online). (a) Temperature variations of meson masses in the PQM model. The dotted line and the dash dot line in the rightmost part of the figure represent the temperature variations of m_σ and m_π, respectively, at $\mu = 0$, the dashed line with two dots in the middle part represents m_σ, and the line with the small dash represents the m_π temperature variation at $\mu_{\rm CEP} = 81.02$ MeV; the solid line in the leftmost part of the figure represents m_σ while the line with thinner dash denotes the m_π temperature variation at $\mu = 305$ MeV. (b) Temperature variations of m_σ and m_π under the influence of fermionic vacuum fluctuations for the PQMVT model computations. Lines represent the same mass variations as in the left panel of the figure. In the PQMVT model, $\mu_{\rm CEP} = 295.22$ MeV.

and π degrees of freedom are not the dynamical fields and are described as collective $q\bar{q}$ excitations in the model. The poles of the quark-antiquark scattering amplitude give the σ and π masses, which can be computed, for example, in the random phase approximation [73]. It is known that the σ mass becomes zero at the critical end point in the sigma model, whereas in the NJL model it always remains a massive mode [25,45].

Finally, we investigate the effect of the fermionic vacuum correction on the emergence of the mass degeneration trend in m_σ and m_π as the chiral-symmetry restoration takes place in the presence of the Polyakov loop potential. Figure 10(a) presents temperature variations of the meson masses at $\mu = 0$, $\mu = \mu_{\rm CEP}$, and $\mu > \mu_{\rm CEP}$ in the PQM model calculations, while Fig. 10(b) shows the corresponding mass variations in the PQMVT model. Since the temperature axis chiral crossover at $\mu = 0$ becomes very sharp and rapid in the PQM model due to the effect of the Polyakov loop potential, the m_σ and m_π temperature variations also show a very sharp and fast mass degeneration at $\mu = 0$ in Fig. 10(a). The mass degeneration for the m_σ and m_π temperature variations at $\mu = 0$ in Fig. 10(b) becomes very smooth due to the effect of fermionic vacuum fluctuations in the PQMVT model, and the temperature for this mass degeneration is highest when we compare it with the values obtained in other models. This is the consequence of the combined effect of the Polyakov loop potential and the fermionic vacuum correction. We point out that the sigma meson mass does not vanish completely at the CEP, as shown in Figs. 10(a) and 10(b), respectively, for the PQM and PQMVT model temperature variations. The temperature variation of m_σ in Fig. 10(a) represented by the dash double dot line,reaches the minimum of about 128 MeV in the PQM model, while the minimum in the temperature variation of m_σ occurs at 76.0 MeV in the PQMVT model computation, as is evident from the dash double dot line in Fig. 10(b). This means that the effective potential of the PQM and PQMVT models do not completely flatten in the radial direction at the CEP. The possible explanation for this might be the coupling/mixing of the chiral order parameter with the Polyakov loop order parameter, which implicitly affects the shape of the effective potential at its minimum. The double derivative of the effective potential (which gives m_σ) with respect to the chiral σ field is also affected in turn. Being the other scalar field in the problem, the Polyakov loop expectation value seems to hamper the complete flattening of the PQM model effective potential when it is plotted only with respect to the σ field in the radial direction at the CEP. In the PQMVT model, this effect seems to be considerably remedied by the presence of the fermionic vacuum term and the minimum value of m_σ becomes 76.0 MeV in its temperature variation. We have also shown the first-order discontinuities in mass evolutions in Figs. 10(a) and 10(b), respectively, for the PQM and PQMVT model computations when $\mu > \mu_{\rm CEP} = 305$ MeV.

IV. SUMMARY AND CONCLUSION

In the present work, we computed the phase diagram for the two-quark-flavor models QMVT, PQMVT, QM, and PQM, and found the CEP positions in the μ and T plane for the explicitly broken chiral symmetry with actual pion mass. Since the PQMVT and QMVT models have become QCD-like due to the fermionic vacuum correction and they yield the second-order transition at $\mu = 0$ on the temperature axis, we also located the TCP in these models for the chiral limit of $m_\pi = 0$. We then plotted the contours of appropriately normalized constant quark number susceptibility and scalar susceptibility around the CEP in different

model scenarios. In order to investigate the qualitative as well as quantitative effects of the fermionic vacuum term and the Polyakov loop potential on the critical behavior around the CEP, we compared the shape and size of these contours in different model calculations. We quantified the proximity of the TCP to the CEP for the QMVT and PQMVT model calculations because the presence or absence of the TCP and its distance from the CEP in the phase diagram significantly influences the nature of criticality around the CEP. Further, we computed and compared the critical exponents resulting from the divergence of the quark number susceptibility at the CEP in different model scenarios. We discussed the possible influence of the TCP on the critical behavior around the CEP. Finally, we plotted the temperature variation of the σ and π meson masses at $\mu = 0$, $\mu = \mu_{\mathrm{CEP}}$, and $\mu > \mu_{\mathrm{CEP}}$ in different models and compared the emerging mass degeneration trend in the σ and π meson mass variations as the chiral symmetry is restored at higher temperatures.

The QMVT model CEP ($T_{\mathrm{CEP}} = 32.24$ MeV, $\mu_{\mathrm{CEP}} = 299.35$ MeV) shifts to $T_{\mathrm{CEP}} = 83.0$ MeV, $\mu_{\mathrm{CEP}} = 295.217$ MeV in the PQMVT model computations, while the QM model CEP ($T_{\mathrm{CEP}} = 102.09$ MeV, $\mu_{\mathrm{CEP}} = 151.7$ MeV) shifts to $T_{\mathrm{CEP}} = 166.88$ MeV, $\mu_{\mathrm{CEP}} = 81.02$ MeV in the PQM model. We thus conclude that the CEP shifts to higher temperatures and lower chemical potentials in the phase diagram due to the effect of the Polyakov loop potential, and that the first-order transition becomes stronger, giving rise to an increased length of the first-order line and a longer region of phase coexistence. On the other hand, the strength of the phase transition becomes weaker due to fluctuations. We find a considerably significant shift of the CEP to larger chemical potentials and smaller temperatures if we compare the respective locations of the CEP in the QMVT and PQMVT model computations to the positions of the CEP obtained, respectively, in the QM and PQM model calculations. This finding leads us to the conclusion that the fermionic vacuum fluctuation does have a very robust influence on the effective potential of QMVT and PQMVT models. It makes the first-order transition significantly weaker and a lot smoother. As a consequence, the first-order line decreases significantly, giving rise to a strong shrinkage of the phase coexistence region in the phase diagram. We find the TCP at $T_t = 133.5$ MeV and $\mu_t = 245.34$ MeV in the chiral-limit ($m_\pi = 0$) computations of the PQMVT model. The QMVT model TCP is found at $T_t = 69.06$ MeV and $\mu_t = 263.0$ MeV. The normalized quark number susceptibility ($R_q = 2$) contour plots around the CEP quantify the proximity of the TCP to the CEP. We find that the TCP location is well inside the $R_q = 2$ contour in the phase diagram of both the QMVT and PQMVT models.

The quark number susceptibilities and scalar susceptibilities diverge at the CEP and are significantly enhanced in its vicinity. Around the CEP in the μ and T plane we plotted contours of the normalized quark number susceptibility for $R_q = 2$, 3, and 5, as well as the normalized scalar susceptibility for the ratios $R_s = 10$, 15, and 25. Since the chiral crossover becomes sharper due to the effect of the Polyakov loop potential, the critical region in the T direction gets significantly compressed in the PQM model (R_q) contours when compared with the pure QM model contours. We infer from the shapes of the QMVT and PQMVT model contours for $R_q = 2$, 3, and 5 that the size of the critical region is increased in a direction perpendicular to the crossover line due to the influence of the fermionic vacuum fluctuations. This effect is less pronounced in the PQMVT model because of the compression of the critical region width due to the presence of the Polyakov loop potential. Further, the extent and size of the critical region in the PQMVT model is noticeably larger in both the μ and T directions compared to that of the QMVT model results. In the PQM model the $R_s = 10$ contour shape is rather compressed in comparison to the pure QM model contour. We do not find the $R_s = 25$ contour in the PQM model, and the $R_s = 15$ contour size is also very thin and insignificantly small because the m_σ falls very rapidly and sharply from 500 MeV to the minimum value of 128 MeV. Since the m_σ variation in the QM model is smoother and its minimum approaches zero, we have found all contours with well-defined sizes for $R_s = 10$, 15, and 25. The R_s contours are also broader in the direction perpendicular to the crossover line, and the critical region gets elongated in the phase diagram and χ_σ is enhanced in the direction parallel to the first-order transition line due to the fermionic vacuum fluctuation. The influence of the fermionic vacuum fluctuation on the criticality around the CEP is quite robust and it is opposite to that of the Polyakov loop potential. This gives a typical shape to the quark number susceptibility and the scalar susceptibility contours in the PQMVT model. When under the influence of only fermionic vacuum fluctuations, the χ_σ contours in the pure QMVT model are broader and rounded.

We further explored the nature of criticality by computing the critical exponents for the divergence of the quark number susceptibility χ_q in the QM, PQM, QMVT, and PQMVT models. We found the critical exponent $\epsilon = 0.6379 \pm 0.0002$ if we approach the μ_{CEP} from the lower-μ side in the QM model, while the critical exponent is $\epsilon = 0.6648 \pm 0.0001$ when the μ_{CEP} is approached from the higher-μ side. The scaling starts around $\log|\mu\text{-}\mu_{\mathrm{CEP}}| < -.5$ in both cases. These exponents show good agreement with the mean-field prediction $\epsilon = 2/3$. We find similar critical exponents for the PQM model, and the effect of the Polyakov loop potential is negligible. If we approach the μ_{CEP} in the QMVT model from the lower-μ side, we find a critical exponent $\epsilon = m = 0.720 \pm 0.00005$, which is noticeably larger than in the QM model. In the QMVT model phase diagram, we have found the

TCP in the chiral limit, which is located well inside the $R_q = 2$ contour surrounding the CEP due to the significant influence of the fermionic vacuum fluctuation. This larger critical exponent is the consequence of the modification of criticality around the CEP due to the presence of the TCP in its proximity. The scaling starts earlier when $\log|\mu\text{-}\mu_{\rm CEP}| < 0.0$, and we observe scaling over several orders of magnitude. We obtain a smaller critical exponent $\epsilon = 0.6938 \pm 0.0001$ when the $\mu_{\rm CEP}$ is approached from the higher-μ side in the PQMVT model. The presence of the Polyakov loop compresses the width of the critical region in the PQMVT model, but its effect on critical exponents is negligible. The value of the critical exponents in the PQMVT model are almost similar to the QMVT model values.

Comparing the temperature variations of meson masses in all four models, we conclude that the mass degeneration in m_σ and m_π at $\mu = 0$ becomes very smooth in the QMVT model, and smoother in the PQMVT model (though less smooth than the QMVT model), and it takes place at a higher temperature. The sharpest and fastest mass degeneration at $\mu = 0$ occurs in the PQM model due to the effect of the Polyakov loop potential, and it is less sharp in the QM model. It is rendered very smooth in the QMVT model and smoother in the PQMVT model, again due to the fact that the strength of the transition becomes quite weak in the presence of the fermionic vacuum term. We found that the sigma mass almost vanishes at $\mu = \mu_{\rm CEP}$ in both the QM and QMVT models, as expected. But the sigma meson mass does not vanish completely at $\mu = \mu_{\rm CEP}$ in the PQM and PQMVT model temperature variations. In the PQM model, m_σ in its temperature variation reaches the minimum value of 128.0 MeV. The Polyakov loop expectation value is another scalar field which gets coupled/mixed with the chiral σ field, and this effect seems to hamper the complete flattening of the PQM model effective potential at the minimum in the radial direction (i.e., the direction of only the σ field at the CEP). In the PQMVT model, this effect seems to be considerably remedied by the presence of the fermionic vacuum term and we get a minimum in the m_σ temperature variation at 76.0 MeV. We have also shown the discontinuities in the mass evolutions, which signal a first-order phase transition at small temperatures when $\mu > \mu_{\rm CEP} = 305$ MeV in all of the models.

ACKNOWLEDGMENTS

Valuable suggestions and computational help from Rajarshi Ray during the completion of this work are specially acknowledged. I am also thankful to Krysztof Redlich for fruitful discussions during the visit to ICPAQGP-2010 at Goa in India. Lot of thanks to Rajarshi Tiwari for helping me in generating good-quality colored figures. General physics discussions with Ajit Mohan Srivastava were very helpful. The computational support of the computing facility developed by the Nuclear Particle Physics group of the Physics Department, Allahabad University, under the Center of Advanced Studies (CAS) funding of UGC, India, is also acknowledged.

[1] D. H. Rischke, Prog. Part. Nucl. Phys. **52**, 197 (2004).
[2] H. Meyer-Ortmanns, Rev. Mod. Phys. **68**, 473 (1996).
[3] B. Muller, Rep. Prog. Phys. **58**, 611 (1995).
[4] L. D. McLerran and B. Svetitsky, Phys. Rev. D **24**, 450 (1981); B. Svetitsky, Phys. Rep. **132**, 1 (1986).
[5] A. M. Polyakov, Phys. Lett. **72B**, 477 (1978).
[6] R. D. Pisarski, Phys. Rev. D **62**, 111501(R) (2000).
[7] B. Layek, A. P. Mishra, A. M. Srivastava, and V. K. Tiwari, Phys. Rev. D **73**, 103514 (2006).
[8] A. A. Khan *et al.*, Phys. Rev. D **64**, 074510 (2001).
[9] F. Karsch, Lect. Notes Phys. **583**, 209 (2002).
[10] P. de Forcrand and O. Philipsen, Nucl. Phys. **B642**, 290 (2002).
[11] Z. Fodor and S. D. Katz, Phys. Lett. B **534**, 87 (2002); Z. Fodor, S. D. Katz, and K. K. Szabo, Phys. Lett. B **568**, 73 (2003).
[12] C. R. Allton, S. Ejiri, S. J. Hands, O. Kaczmarek, F. Karsch, E. Laermann, and C. Schmidt, Phys. Rev. D **68**, 014507 (2003); C. R. Allton, M. Doring, S. Ejiri, S. J. Hands, O. Kaczmarek, F. Karsch, E Laermann, and K. Redlich, Phys. Rev. D **71**, 054508 (2005).
[13] Y. Aoki, Z. Fodor, S. D. Katz, and K. K. Szabo, Phys. Lett. B **643**, 46 (2006); Y. Aoki, S. Borsányi, S. Dürr, Z. Fodor, S. D. Katz, S. Krieg, and K. Szabo, J. High Energy Phys. 06 (2009) 088.
[14] F. Karsch, J. Phys. G **31**, S633 (2005).
[15] F. Karsch, arXiv:0701.210.
[16] M. Cheng *et al.*, Phys. Rev. D **74**, 054507 (2006).
[17] M. Cheng *et al.*, Phys. Rev. D **77**, 014511 (2008).
[18] S. Digal, E. Laermann, and H. Satz, Eur. Phys. J. C **18**, 583 (2001).
[19] A. Bazavov *et al.*, Phys. Rev. D **85**, 054503 (2012); S. Borsanyi, Z. Fodor, C. Hoelbling, S. D. Katz, S. Krieg, C. Ratti, and K. K. Szabó, J. High Energy Phys. 09 (2010) 073.
[20] R. D. Pisarski and F. Wilczek, Phys. Rev. D **29**, 338 (1984).
[21] M. Asakawa and K. Yazaki, Nucl. Phys. **A504**, 668 (1989).
[22] A. Barducci, R. Casalbuoni, S. De Curtis, R. Gatto, and G. Pettini, Phys. Lett. B **231**, 463 (1989); Phys. Rev. D **41**, 1610 (1990).
[23] J. Berges and K. Rajagopal, Nucl. Phys. **B538**, 215 (1999).

[24] Y. Hatta and T. Ikeda, Phys. Rev. D **67**, 014028 (2003).
[25] H. Fujii, Phys. Rev. D **67**, 094018 (2003).
[26] K. Fukushima, Phys. Part. Nucl. Lett. **8**, 838 (2011).
[27] D. T. Son and M. A. Stephanov, Phys. Rev. D **70**, 056001 (2004); Y. Aoki, G. Androdi, Z. Fodor, S. D. Katz, and K. K. Szabo, Nature (London) **443**, 675 (2006); S. Gupta, X. Luo, B. Mohanty, H. G. Ritter, and N. Xu, Science **332**, 1525 (2011).
[28] O. Philipsen, arXiv:1111.5370.
[29] E. S. Bowman and J. I. Kapusta, Phys. Rev. C **79**, 015202 (2009); J. I. Kapusta and E. S. Bowman, Nucl. Phys. **A830**, 721c (2009).
[30] L. Ferroni, V. Koch, and M. B. Pinto, Phys. Rev. C **82**, 055205 (2010).
[31] M. A. Stephanov, K. Rajagopal, and E. V. Shuryak, Phys. Rev. D **60**, 114028 (1999); Phys. Rev. Lett. **81**, 4816 (1998).
[32] S. Jeon and V. Koch, Phys. Rev. Lett. **85**, 2076 (2000); in *Quark Gluon Plasma*, edited by R. C. Hwa (World Scientific, Singapore, 2004), p. 430.
[33] S. Ejiri, F. Karsch, and K. Redlich, Phys. Lett. B **633**, 275 (2006).
[34] J. Adams *et al.* (STAR Collaboration), Nucl. Phys. **A757**, 102 (2005); M. Aggarwal *et al.* (STAR Collaboration), Phys. Rev. Lett. **105**, 022302 (2010).
[35] B. Mohanty, Nucl. Phys. **A830**, 899c (2009).
[36] V. Koch, arXiv:0810.2520.
[37] X. Luo, B. Mohanty, H. G. Ritter, and N. Xu, Phys. At. Nucl. **75**, 676 (2012).
[38] J. T. Lenaghan, D. H. Rischke, and J. Schaffner-Bielich, Phys. Rev. D **62**, 085008 (2000); J. T. Lenaghan and D. H. Rischke, J. Phys. G **26**, 431 (2000).
[39] S. Chiku and T. Hatsuda, Phys. Rev. D **58**, 076001 (1998).
[40] S. Chiku, Prog. Theor. Phys. **104**, 1129 (2000).
[41] T. Herpay, A. Patkós, Z. Szép, and P. Szépfalusy, Phys. Rev. D **71**, 125017 (2005).
[42] T. Herpay and Z. Szép, Phys. Rev. D **74**, 025008 (2006).
[43] P. Kovács and Z. Szép, Phys. Rev. D **75**, 025015 (2007).
[44] G. Fejos and A. Patkos, Phys. Rev. D **82**, 045011 (2010).
[45] O. Scavenius, A. Mocsy, I. N. Mishustin, and D. H. Rischke, Phys. Rev. C **64**, 045202 (2001).
[46] B. J. Schaefer and M. Wagner, Phys. Rev. D **79**, 014018 (2009).
[47] J. O. Andersen, R. Khan, and L. T. Kyllingstad, arXiv:1102.2779; R. Khan and L. T. Kyllingstad, AIP Conf. Proc. **1343**, 504 (2011).
[48] A. Jakovac, A. Patkos, Z. Szep, and P. Szepfalusy, Phys. Lett. B **582**, 179 (2004).
[49] A. Mocsy, I. N. Mishustin, and P. J. Ellis, Phys. Rev. C **70**, 015204 (2004).
[50] B.-J. Schaefer and J. Wambach, Nucl. Phys. **A757**, 479 (2005).
[51] B.-J. Schaefer and J. Wambach, Phys. Rev. D **75**, 085015 (2007).
[52] P. Kovacs and Z. Szep, Phys. Rev. D **75**, 025015 (2007).
[53] A. Jakovac and Z. Szep, Phys. Rev. D **82**, 125038 (2010).
[54] P. Costa, M. C. Ruivo, and C. A. de Sousa, Phys. Rev. D **77**, 096001 (2008).
[55] J.-L Kneur, M. B. Pinto, and R. O. Ramos, Phys. Rev. C **81**, 065205 (2010).
[56] T. Kahara and K. Tuominen, Phys. Rev. D **78**, 034015 (2008); **80**, 114022 (2009); **82**, 114026 (2010).
[57] D. Nickel, Phys. Rev. D **80**, 074025 (2009).
[58] K. Fukushima, Phys. Lett. B **591**, 277 (2004).
[59] C. Ratti, M. A. Thaler, and W. Weise, Phys. Rev. D **73**, 014019 (2006).
[60] S. Rößner, C. Ratti, and W. Weise, Phys. Rev. D **75**, 034007 (2007).
[61] S. Rößner, T. Hell, C. Ratti, and W. Weise, Nucl. Phys. **A814**, 118 (2008).
[62] S. K. Ghosh, T. K. Mukherjee, M. G. Mustafa, and R. Ray, Phys. Rev. D **73**, 114007 (2006).
[63] C. Sasaki, B. Friman, and K. Redlich, Phys. Rev. D **75**, 074013 (2007).
[64] T. Hell, S. Rößner, M. Cristoforetti, and W. Weise, Phys. Rev. D **79**, 014022 (2009).
[65] H. Abuki, R. Anglani, R. Gatto, G. Nardulli, and M. Ruggieri, Phys. Rev. D **78**, 034034 (2008).
[66] M. Ciminale, R. Gatto, N. D. Ippolito, G. Nardulli, and M. Ruggieri, Phys. Rev. D **77**, 054023 (2008).
[67] W.-J. Fu, Z. Zhang, and Y.-X. Liu, Phys. Rev. D **77**, 014006 (2008).
[68] K. Fukushima, Phys. Rev. D **77**, 114028 (2008).
[69] K. Fukushima, Phys. Rev. D **78**, 114019 (2008).
[70] K. Fukushima, Phys. Rev. D **79**, 074015 (2009).
[71] H. Hansen, W. M. Alberico, A. Beraudo, A Molinari, M. Nardi, and C. Ratti, Phys. Rev. D **75**, 065004 (2007).
[72] P. Costa, M. C. Ruivo, C. A. de Sousa, H. Hansen, and W. M. Alberico, Phys. Rev. D **79**, 116003 (2009).
[73] S. P. Klevansky, Rev. Mod. Phys. **64**, 649 (1992).
[74] K. Kashiwa, H. Kouno, M. Matsuzaki, and M. Yahiro, Phys. Lett. B **662**, 26 (2008).
[75] A. E. Radzhabov, D. Blaschke, M. Buballa, and M. K. Volkov, Phys. Rev. D **83**, 116004 (2011).
[76] O. Lourenco, M. Dutra, T. Frederico, A. Delfino, and M. Malheiro, Phys. Rev. D **85**, 097504 (2012); O. Lourenco, M. Dutra, A. Delfino, and M. Malheiro, Phys. Rev. D **84**, 125034 (2011).
[77] B. J. Schaefer, J. M. Pawlowski, and J. Wambach, Phys. Rev. D **76**, 074023 (2007).
[78] B. J. Schaefer and M. Wagner, in The Proceedings of the 30th International School of Nuclear Physics Erice, Italy, 2008 (to be published).B. J. Schaefer and M. Wagner, arXiv:0812.2855.
[79] B. J. Schaefer, M. Wagner, and J. Wambach, Proc. Sci., CPOD2009 (2009) 017.
[80] B. J. Schaefer, M. Wagner, and J. Wambach, Phys. Rev. D **81**, 074013 (2010).
[81] H. Mao, J. Jin, and M. Huang, J. Phys. G **37**, 035001 (2010).
[82] U. S. Gupta and V. K. Tiwari, Phys. Rev. D **81**, 054019 (2010).
[83] G. Marko and Z. Szep, Phys. Rev. D **82**, 065021 (2010).
[84] V. Skokov, B. Friman, E. Nakano, K. Redlich, and B.-J. Schaefer, Phys. Rev. D **82**, 034029 (2010).
[85] T. K. Herbst, J. M. Pawlowski, and B.-J. Schaefer, Phys. Lett. B **696**, 58 (2011).
[86] A. Barducci, R. Casalbuoni, G. Pettini, and R. Gatto, Phys. Rev. D **49**, 426 (1994).

[87] M. A. Halasz, A. D. Jackson, R. E. Shrock, M. A. Stephanov, and J. J. M. Verbaarschot, Phys. Rev. D **58**, 096007 (1998).
[88] M. Harada and A. Shibata, Phys. Rev. D **59**, 014010 (1998).
[89] N. Brouzakis and N. Tetradis, Nucl. Phys. **A742**, 144 (2004).
[90] C. Nonaka and M. Asakawa, Phys. Rev. C **71**, 044904 (2005).
[91] H. Fujii and M. Ohtani, Phys. Rev. D **70**, 014016 (2004).
[92] P. Costa, C. A. de Sousa, M. C. Ruivo, and H. Hansen, Europhys. Lett. **86**, 31001 (2009); P. Costa, M. C. Ruivo, C. A. de Sousa, and H. Hansen, Symmetry **2**, 1338 (2010).
[93] G. A. Contrera, M. Orsaria, and N. N. Scoccola, Phys. Rev. D **82**, 054026 (2010).
[94] A. J. Mizher, M. N. Chernodub, and E. S. Fraga, Phys. Rev. D **82**, 105016 (2010).
[95] L. F. Palhares and E. S. Fraga, Phys. Rev. D **78**, 025013 (2008).
[96] E. S. Fraga, L. F. Palhares, and M. B. Pinto, Phys. Rev. D **79**, 065026 (2009).
[97] L. F. Palhares and E. S. Fraga, Phys. Rev. D **82**, 125018 (2010).
[98] U. S. Gupta and V. K. Tiwari, Phys. Rev. D **85**, 014010 (2012).
[99] B.-J. Schaefer and M. Wagner, Phys. Rev. D **85**, 034027 (2012).
[100] S. Chatterjee and K. A. Mohan, Phys. Rev. D **85**, 074018 (2012).
[101] M. Quiros, in *Proceeding: The Summer School in High Energy Physics and Cosmology, ICTP Series in Theoretical Physics, Trieste, Italy, 1998*, edited by A. Masiero, G. Senjanovic, and A. Smirnov (World Scientific, Singapore, 1999), Vol. 15, p. 436.
[102] R. B. Griffiths and J. Wheeler, Phys. Rev. A **2**, 1047 (1970).